X-ray diffraction study of Co-Cu superlattices

2000 J. Phys.: Condens. Matter 12 6755

(http://iopscience.iop.org/0953-8984/12/30/307)

J. Phys.: Condens. Matter **12** (2000) 6755–6771. Printed in the UK PII: S0953-8984(00)14083-4

X-ray diffraction study of Co–Cu superlattices

A Y Babkevich†, R A Cowley†, P Goddard†, R Schlinkert†, B M Murphy‡, S P Collins‡ and B J Hickey§

† Clarendon Laboratory, Oxford University, Parks Road, Oxford OX1 3PU, UK
‡ Daresbury Laboratory, CLRC, Warrington WA4 4AD, UK
§ Department of Physics, University of Leeds, Leeds LS2 9JT, UK

Received 22 May 2000

Abstract. Epitaxial Co/Cu superlattices were grown by molecular beam epitaxy on sapphire substrates and investigated by high-resolution x-ray diffraction at room temperature. Detailed analysis of x-ray scattering along the $[10.L]$ reciprocal-lattice rows revealed that about 80% of Co was hexagonal close packed (h.c.p.) and only 20% was face-centred cubic (f.c.c.). A combination of modelling of x-ray scattering from superlattices with measurements of coherence lengths of individual components of the scattering suggests that the f.c.c. Co grows as a single block at the beginning of Co layers and the growth presumably starts from islands rather than from continuous Co layers. The h.c.p. structure is one-dimensionally disordered by stacking faults which appear after approximately every 12 layers of Co on average. Upon heating in ultrahigh vacuum to 700 °C the coherent superlattice structure was completely destroyed and the resulting structure consisted of relaxed layers of Co and Cu.

(Some figures in this article are in colour only in the electronic version; see `www.iop.org`)

1. Introduction

The giant magnetoresistance (GMR) in multilayers is a subject of intensive investigation because of the possibility of its application to field-sensing devices such as magnetic readout heads, magnetic sensors and other information storage and retrieval devices. Due to their large GMR, up to 80% at room temperature [1, 2], Co/Cu multilayers have been receiving considerable attention from scientists and engineers [3–24]. While the general principles of the GMR are known, there is still a lack of understanding of the factors that control the magnitude of the effect. Strong evidence exists that interface scattering of electrons and fluctuations of spins at the interface play a key role in determining the GMR effect [25–27]. The structure of Co/Cu multilayers and interfaces is able to provide an explanation of some of the magnetic properties of this system [15–22]. However, the structural features responsible for the GMR have yet to be identified.

It is therefore important to know, for example, the structural state of Co layers in multilayers. Cobalt epitaxially grown on the Cu(111) surface typically has either the face-centred cubic (f.c.c.) or the hexagonal close-packed (h.c.p.) structure. The structure of the Co layer affects the structure of the Co/Cu interface and also the volume ratio of f.c.c. and h.c.p. Co which may have a strong effect on the magnetization easy axis due to a big difference between the magnetocrystalline anisotropy of h.c.p. and f.c.c. Co. The growth of Co on Cu has been studied in different ways [3–12, 28]. Despite partly conflicting reports about the growth of the first few layers, it seems to be generally accepted that the f.c.c. structure dominates in the first

0953-8984/00/306755+17$30.00

few monolayers of Co, while the h.c.p. structure tends to develop with increasing Co layer thickness. Furthermore the growth that takes place for Cu on Co is different from that of Co on Cu. The Cu does not follow the Co's h.c.p. stacking but grows with an f.c.c. stacking sequence from the very beginning [14].

The structure of real superlattices is disordered and the effect of disorder is of crucial importance for understanding the different physical properties and enabling the potential of electronic devices to be realized. Significant effort has been made to characterize, mostly by x-ray diffraction, such structural imperfections in SLs as interfacial roughness, interdiffusion, imperfect crystallinity and crystalline misorientation [6, 13, 18, 20, 23, 24, 29–32]. A problem which remains open is that of the degree of perfection of the structure of Co in multilayers with respect to one-dimensional (1-D) (stacking) disorder and the effect of this disorder on the magnetic properties. Stacking disorder is particularly important for Co [33–35] because it has a much lower (3.1×10^{-2} J m^{-2} or less) stacking fault energy than Cu (7.0×10^{-2} J m^{-2}) [36–38]. Furthermore, cobalt may also change its low-temperature crystal structure from h.c.p. (2H) to a highly correlated 1-D disordered structure if it is alloyed with a very small amount of Cu [39]. From a technological point of view it is desirable to have low stacking disorder because the GMR is reduced when stacking faults develop in the cobalt layer [12, 15]. A detailed knowledge of the stacking of atomic planes in Co/Cu multilayers is therefore required.

The present paper reports the results of a high-resolution x-ray diffraction study of two Co/Cu superlattices (SLs), prepared by molecular beam epitaxy (MBE). A quantitative analysis of the x-ray diffraction data allows us to characterize the structure of the SLs and to identify the different stackings of close-packed planes inside the Co and Cu layers of the superlattice. Firstly we show that direct computation of the intensities on a grid of parameters is more appropriate for characterizing a SL structure than the commonly used least-squares method. Using x-ray scattering and computer simulation we have found the lattice spacings of Co and Cu, the size of the blocks of each material and the width of a Co/Cu interface in the SLs. We have also established that

(i) 80% of Co in both SLs has the h.c.p. structure, despite a big difference (by a factor of 2) in the size of the Co blocks,
(ii) the initial stacking of Co layers is f.c.c., and that f.c.c. Co grows in islands rather than as a continuous layer,
(iii) the h.c.p. Co is 1-D disordered by random SFs occurring approximately every 12th close-packed plane on average.

After a discussion of the sample preparation and the experimental x-ray technique the paper describes the computational technique. The method is tested for a Dy/Lu superlattice and produces excellent agreement between the measured and calculated intensities both for the [00L] and [10L] reflections confirming an absence of stacking disorder in this system (section 3). The next section describes the detailed quantitative characterization of the structure of two Co/Cu SLs. Comparison of the measured x-ray data with the diffraction patterns simulated by various models is given in section 4. The effect of heat treatment (fast heating in UHV to 700 °C followed by slow 1 °C min^{-1} cooling to 20 °C) on the Co/Cu SL structure is discussed in section 5. The last section (section 6) gives a brief summary of the results and concluding remarks.

2. Sample growth and experimental techniques

Two single-crystalline Co/Cu(111) SLs were grown using the molecular-beam-epitaxy (MBE) facility, at the University of Leeds. To ensure good epitaxy and an atomically smooth surface

of the superlattices a 20 nm thick Nb buffer layer was grown on the $(11\bar{2}0)$ plane of a sapphire substrate at 900 °C. It was followed by a 20 nm Au seed layer deposited at 200 °C. Fifty bilayers of Cu (5 nm)/Co (5 nm) were then grown with the substrate temperature reduced to 80 °C to minimize the interdiffusion. The growth of the SL was started with a Cu layer to avoid any alloying of the Co with the Nb. The samples were protected from oxidation by either a 1.5 nm or 5 nm Au cap. The epitaxial relations between the Al_2O_3, Nb and Cu have been established [40] for similar superlattices grown on a Cu seed, and the Cu(111) planes are perpendicular to the growth direction.

A Dy/Lu superlattice was grown at a temperature of about 400 °C on a Al_2O_3 substrate by MBE in Oxford. A 17 nm Nb buffer layer and a 100 nm Lu seed were grown on the substrate. A $(Dy/Lu)_{20}$ SL was grown on the seed and then covered with a 10 nm Lu cap. This SL is composed of materials with only a small lattice mismatch (<2%) and so is similar in this respect to Co/Cu SLs.

The measurements of the x-ray scattering were made with a triple-crystal diffractometer in Oxford (Cu Kα radiation with a wavelength $\lambda = 0.154\,051$ nm, Ge monochromator and crystal analyser) and with station 16.3 at the Daresbury Laboratory ($\lambda = 0.1$ nm, Si monochromator and analyser). The samples were mounted with the hexagonal $\boldsymbol{a}^*/\boldsymbol{c}^*$-directions in the scattering plane defined by the reciprocal-lattice vectors

$$|\boldsymbol{a}^*_{hex}| = \frac{2\pi}{d_{11\bar{2}_{\text{f.c.c.}}}} = \frac{2\pi}{d_{100_{\text{h.c.p.}}}} \qquad |\boldsymbol{c}^*_{hex}| = \frac{2\pi}{d_{111_{\text{f.c.c.}}}} = \frac{2\pi}{d_{002_{\text{h.c.p.}}}}.$$

Radial ($\theta/2\theta$) x-ray scans with the scattering vector $Q = 4\pi \sin(\theta)/\lambda$ perpendicular to the SL growth direction show satellite reflections centred near the (111) and (222) reflections of Co and Cu testifying that there is a Co/Cu(111) SL. The position of the main SL reflections corresponds to an averaged plane spacing $\overline{d}$ in the growth direction and is equal to $2\pi/\overline{d}$. The spacing between the SL peaks is determined by the average thickness $\overline{L}$ of a Cu/Co bilayer and is $\Delta q = 2\pi/\overline{L}$. For convenience, the SL peak positions are often indexed with respect to the main peak as

$$Q_p = \frac{2\pi}{\overline{d}} + \frac{2\pi}{\overline{L}}p$$

where $p = 0, \pm1, \pm2, \ldots$ is the integer index of the peak. These radial scans are typically used to characterize the structure of SLs in different systems. However, they do not contain information about the stacking of lattice planes and so cannot distinguish between the f.c.c. and h.c.p. structures.

Both f.c.c. and h.c.p. structures may be formally considered as the stacking of identical close-packed planes, $(111)_{\text{f.c.c.}}$ or $(001)_{\text{h.c.p.}}$ (figure 1). The positions of the atoms are determined by the stacking order of the close-packed planes. If the positions of the atoms in the first layer in the sequence are designated by A, as in figure 1(A), the next plane can only occupy either B or C positions, which correspond to two different interstices of the A layer. Any three-dimensional close-packed structure results from a particular stacking of the close-packed planes in the A, B or C position with the restriction that no two successive layers are in an identical position. The identity period of these layer stackings is determined by the number of layers after which the stacking sequence repeats itself. The two simplest arrangements which are periodic, and which can therefore give a crystal lattice, are the h.c.p. ABAB... (BCBC... or CACA... are also h.c.p.), and the f.c.c. ABCABC... [41]. The f.c.c. ACBACB... stacking is the twin of the ABC... f.c.c. lattice. The energy differences between the f.c.c. and h.c.p. structures are small and the orientational relationship between them is $(111)_{\text{f.c.c.}} \parallel (001)_{\text{h.c.p.}}$, $\langle 112\rangle_{\text{f.c.c.}} \parallel \langle 100\rangle_{\text{h.c.p.}}$ [37].

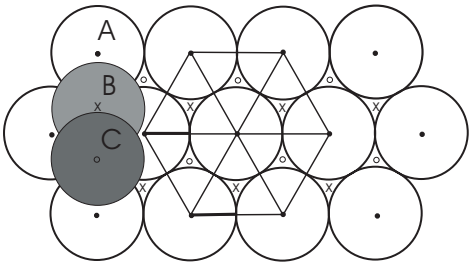

(A)

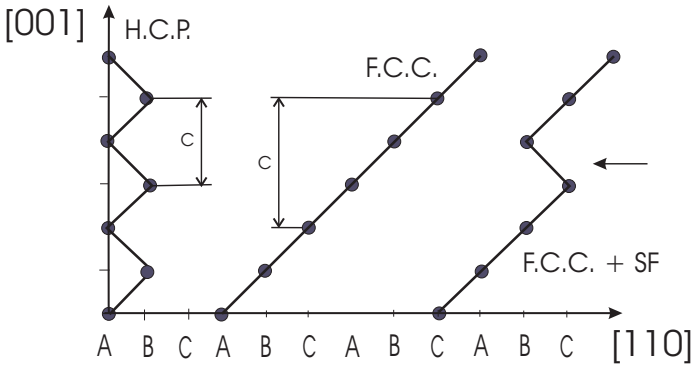

(B)

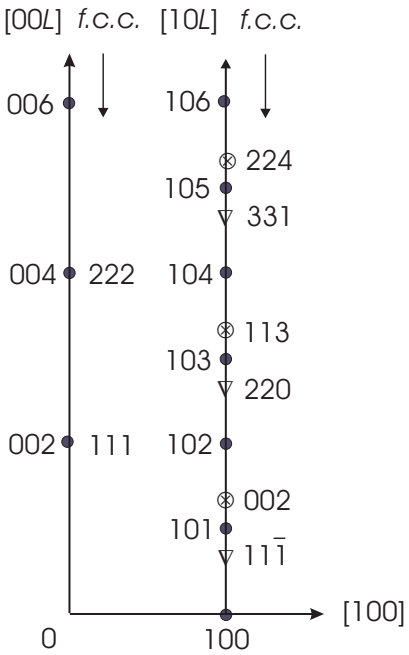

(C)

Figure 1. Layer stacking in close-packed structures and positions of x-ray peaks in diffraction patterns. (A) Closest packing of atoms in $(111)_{\text{f.c.c.}}$ and $(001)_{\text{h.c.p.}}$ planes. (B) Stacking of close-packed planes in h.c.p., f.c.c. and 1-D disordered (with a single SF) crystals. (C) A reciprocal-space map showing respective positions of reflections of the h.c.p. and f.c.c. structures.

The stacking of the planes and in particular the f.c.c. and h.c.p. structures can be studied by x-ray scattering measurements in which the scattering vector is scanned along L with $H - K \neq 0 \bmod 3$ in the h.c.p. notation. In these scans the component of the scattering vector perpendicular to the growth plane is varied while the in-plane component is held fixed. We have varied the scattering vector longitudinally along the $[00L]$ and $[10L]$ directions for the hexagonal structure and transversely through the Bragg reflections in scans parallel to the $[100]_{\text{h.c.p.}}$ direction.

3. Modelling of x-ray scattering from superlattices

The simplest model of a SL assumes an abrupt composition profile with the bulk lattice spacings for each material and does not allow for any fluctuations of the composition, lattice spacing or modulation wavelength. It does not usually give an adequate description of the experimental data, because the diffracted intensities are in fact greatly affected by structural disorder [32, 42–49]. The models for disorder have two aspects: (a) fluctuations of the structural parameters along the growth direction and (b) imperfections of the atomic planes perpendicular to the growth direction and of their stacking. The first kind of disorder arises from fluctuations in the interlayer spacings or in the number of lattice planes in each block of layers or at the interfaces by interdiffusion of materials etc. The second arises, for example, from interfacial roughness, point and linear defects and stacking disorder. In the present study we use a simple structural model that includes the effects of interdiffusion and a smooth change of the $d_{111_{\text{f.c.c.}}}/d_{001_{\text{h.c.p.}}}$ lattice spacing at the interface and we also allow for different stackings of the close-packed planes in the crystal.

The kinematical theory of scattering from the SLs composed of two different materials [50] is one dimensional and takes into account the interdiffusion and the strain in the growth direction but does not deal with any imperfections in the stacking sequence of the close-packed atomic planes. Therefore some extension to the theory was needed to include these changes.

The intensity (structure factor) of the Bragg scattering from the bilayer consisting of n_1 monolayers of material 1 and n_2 layers of material 2 can be written as

$$I(\boldsymbol{Q}) \sim \left| \sum_{N} f_m(\boldsymbol{Q}) \exp(\mathrm{i}\boldsymbol{Q} \cdot \boldsymbol{R}_m) \right|^2 \tag{1}$$

where $\boldsymbol{Q}$ is the scattering vector, $\boldsymbol{R}_m$ is the position of the mth atomic plane, $f_m(\boldsymbol{Q})$ is the scattering amplitude of this plane and $N = n_1 + n_2$ is the total number of atomic planes in the structure. The thickness of each layer in the SL is given by $(n_1 - 1)d_1$ or $(n_2 - 1)d_2$, where d_1 and d_2 are lattice spacings in the c-direction. Layer thickness fluctuations are not included in the model.

In hexagonal coordinates, figure 1, positions of the atoms in any arbitrary regular or 1-D disordered close-packed structure could only take one of three possible values:

$$R_m^{\mathrm{A}} = \left(0, 0, \sum_{l_{\mathrm{A}}} d(l_{\mathrm{A}})\right) \tag{2a}$$

$$R_m^{\mathrm{B}} = \left(\frac{1}{3}a, -\frac{1}{3}a, \sum_{l_{\mathrm{B}}} d(l_{\mathrm{B}})\right) \tag{2b}$$

$$R_m^{\mathrm{C}} = \left(-\frac{1}{3}a, \frac{1}{3}a, \sum_{l_{\mathrm{C}}} d(l_{\mathrm{C}})\right) \tag{2c}$$

where a is an in-phase lattice constant, l_{A}, l_{B} and l_{C} are integers ($0 \leqslant l_{\mathrm{A}}, l_{\mathrm{B}}, l_{\mathrm{C}} \geqslant N - 1$)

specifying the positions of A-, B- and C-type atomic planes in the SL and d is the lattice spacing in the growth direction, i.e. d_{001}.

The d-spacing in the c-direction changes at the boundary between the two materials and the boundary itself is not sharp. The same happens to the scattering amplitudes of the layers. A convenient way of modelling the d_{001}-spacings and the $f_m(\boldsymbol{Q})$ is to express them via a sum of $\tanh(l)$ functions [50] as

$$g_1(l) = \frac{1}{2}\{1 + \tanh(l/\lambda_1) - \tanh[(l - n_1)/\lambda_1] + \tanh[(l - n_1 - n_2)/\lambda_1]\} \tag{3}$$

$$d_{001}(l) = g_1(l)d_1 + [1 - g_1(l)]d_2 \tag{4}$$

$$t_1(l) = \frac{1}{2}\left\{1 + \tanh\left[\left(l + \frac{1}{2}\right)\Big/\lambda_2\right] - \tanh\left[\left(l + \frac{1}{2} - n_1\right)\Big/\lambda_2\right] + \tanh\left[\left(l + \frac{1}{2} - n_1 - n_2\right)\Big/\lambda_2\right]\right\} \tag{5}$$

$$f(Q, l) = t_1(l)f_1(Q) + [1 - t_1(l)]f_2(Q) \tag{6}$$

where λ_1 and λ_2 are widths of the interfaces, f_1, d_1 and f_2, d_2 are the scattering cross-sections and d-spacings of the first and second material, respectively, and l is the number of atomic planes in the bilayer, $0 \leqslant l \leqslant N - 1$. Once the values of d_m and f_m are determined for each atomic plane m, at a given scattering angle, the scattering intensity is calculated using equation (1).

The structure of the superlattice is given by the parameters of the model n_1, n_2, d_1, d_2, λ_1 and λ_2. Initially it seems obvious that the parameters can be obtained from a least-squares fit to the measured scattering profile. Indeed, this method is used in most calculations. Some of the problems with the non-linear least squares fitting are:

(1) the results depend on the initial values of the fitting parameters and sometimes are not reproducible with the different starting values;
(2) it may require fitting of a full diffraction pattern with hundreds or even thousands of points on it;
(3) if parameters n_1 and n_2 are allowed to vary, they may take irrational values which are not consistent with the model.

The procedure which we have used to analyse the scattering from the SLs avoids these complications. The least-squares fit is replaced by the calculation of the x-ray scattering from the SLs on a grid of all of the adjustable parameters of the model. By calculating the intensities for different combinations of parameters and comparing them with the measured intensities, we obtain a model which gives the lowest discrepancy between the measurement and calculation. The best fit is determined by using one of the criteria developed for conventional structure analysis [51]. Calculations show that the best results for the SLs are obtained with the so-called *R-weighted pattern* which is defined as

$$R_{wp} = \left\{\frac{\sum w_i[I_i(\text{meas.}) - I_i(\text{calc.})]^2}{\sum w_i[I_i(\text{meas.})]^2}\right\}^{1/2}. \tag{7}$$

Note that the numerator in equation (7) is minimized in the least-squares method. Here I_i(meas.) and I_i(calc.) are the measured and calculated intensities of a few well-defined SL peaks rather than the intensity at every measured point in the diffraction pattern as minimized in a Rietveld refinement. The intensity of the SL reflections is calculated from the models, multiplied by a scaling factor and compared to the measured values using (7). The best fits are those with the lowest R_{wp} and the lowest difference between the calculated (X_{calc}) and measured (X_{meas}) positions of the peaks. Different weighting schemes have been tested and

the weight coefficients $w_i = [I_i(\text{meas.})]^{-2}$ in equation (7) usually gave models that gave a better account of the weak reflections. The discrepancy in position was evaluated as the mean square deviation σ_{pos} given as

$$\sigma_{pos}^2 = \frac{1}{n}\sum_n (X_{meas}^i - X_{calc}^i)^2. \tag{8}$$

The areas, I_i(meas.), centres and FWHM of the SL peaks are obtained by a least-squares fit of the intensity distribution measured in wave-vector scans with a series of peaks of appropriate shape. In our triple-crystal x-ray measurements, the Pearson VII function usually gives the best fit to the measured reflection profiles, namely

$$P_{VII}(x) = \frac{I_0}{[1 + (x/k)^2]^m} \tag{9}$$

where I_0 is the amplitude and the FWHM is related to the peak width k by FWHM $= 2[2^{1/m} - 1]^{1/2}k$. For $m = 1$, P_{VII} is an exact Lorentzian and as $m \to \infty$ it tends towards a Gaussian line shape. At $m = 50$, the function is essentially Gaussian [52].

As soon as the centres of the SL peaks and the errors in the position of the peaks are known from the experiment, they can be used to constrain the possible values for the parameters. The other useful ratio simplifying the calculations is $n_1 + n_2 - 1 = Q_{p=0}/\Delta q$, where $Q_{p=0}$ is the position of the main SL peak which characterizes the average structure and Δq is the mean measured distance between the centres of the SL peaks.

If the ranges for the parameter values are wide enough that every possibility is considered, the algorithm ensures that there is not a very much better fit elsewhere in parameter space. The efficiency of the computational procedure depends on the number of parameters, step size and computer speed.

3.1. Modelling of a Dy/Lu superlattice

As a demonstration of the capabilities of this method, it was used on a $(Dy_{14}/Lu_{28})_{20}$ superlattice, where the subscripts give the nominal number of layers of each material and total number of bilayer repeats. Figure 2 shows the x-ray intensity measured as the scattering vector varied along the $[00L]$ and $[10L]$ reciprocal-lattice directions. The analysis of the Dy/Lu SL is simplified because both materials have the h.c.p. crystal structure and stacking faults are not expected. The results shown in figure 2 have up to six satellites around the (002) reflection at $Q_{p=0} = 22.539$ nm^{-1} and around the (004) reflection at $Q_{p=0} = 45.064$ nm^{-1}. The peaks at $Q = 22.635$ nm^{-1} and $Q = 45.259$ nm^{-1} are from the Lu seed layer.

Following the procedure described in the previous section the x-ray diffraction profiles around the (002) and (004) reflections were fitted with the P_{VII}-function and the intensities and positions of the SL peaks obtained. These values gave the data required for the calculation of the diffracted intensities on a grid of the parameter values. The two groups of $[00L]$ SL peaks were fitted to the model simultaneously. We allowed a wide range of possible values for n_{Dy}, n_{Lu}, d_{Dy}, d_{Lu} around their nominal values and used a single parameter $\lambda = \lambda_1 = \lambda_2$ to describe the width of the interface which was allowed to vary from 1 to 8 with a step of 0.5. Wide limits for the values of the parameters were taken to make sure that all the adequate models were found.

The program generates structural models which satisfy the values of the peak positions and minimize R_{wp}. The best fit to the data was achieved at $n_1 = 14$, $n_2 = 29$, $d_1 = 2.8401$, $d_2 = 2.7647$ and $\lambda = 3.5$. The parameters of the model were used to plot the intensity profiles from the calculated values of intensities and peak centres (see figure 2). The FWHM and shape (specified by m in equation (9)) of the peaks were fixed at the values found initially from

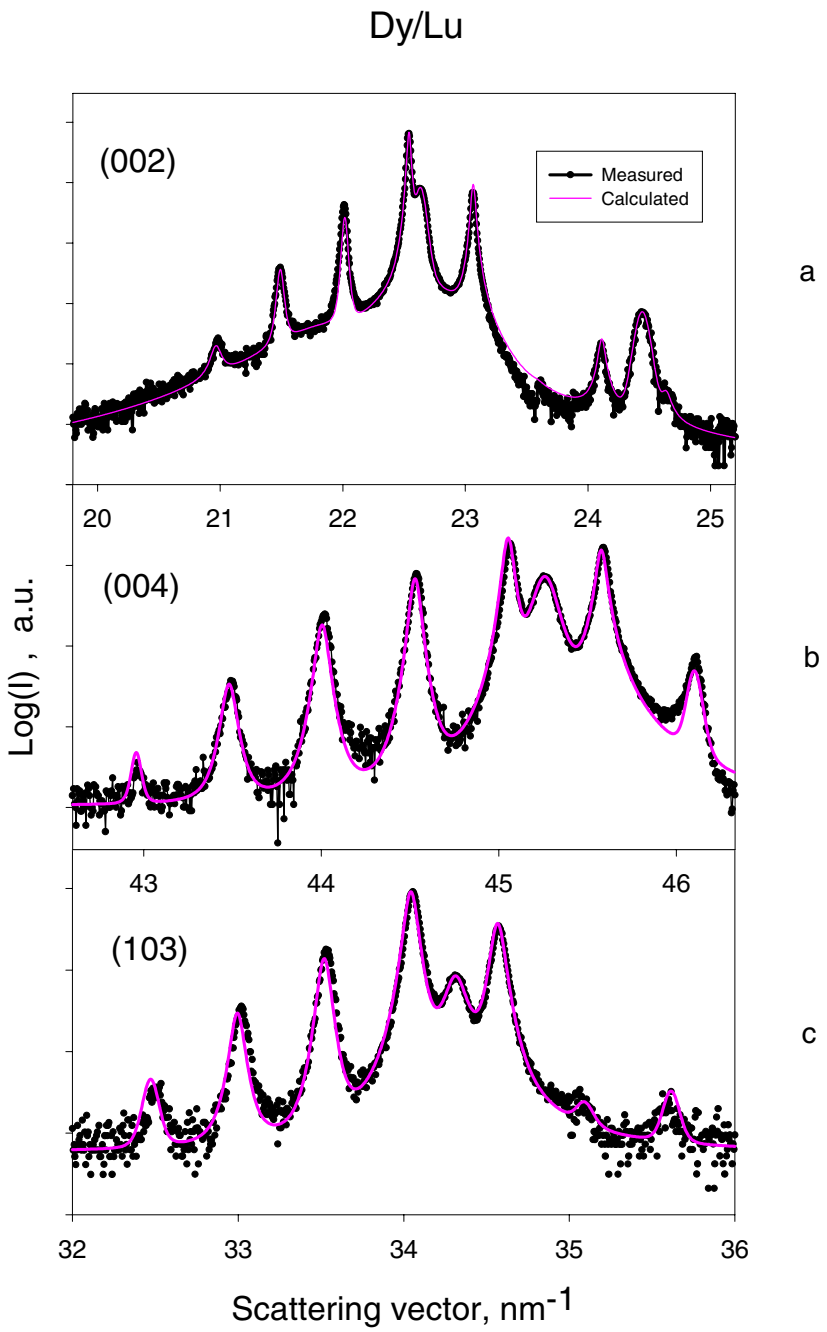

Figure 2. X-ray scattering from a Dy/Lu superlattice. The figure demonstrates the good agreement between the measured and calculated intensities for $[00L]$ ((a), (b)) and $[10L]$ (c) directions in reciprocal space. The latter pattern clearly shows satellite peaks from the superlattice.

the fit to a sum of P_{VII}-functions. Figure 2 shows that the calculated intensities are in good agreement with the measured diffraction patterns in both the $[00L]$ and $[10L]$ directions. Note

that the intensities measured in the $[10L]$ direction were not used to derive the parameters of the SL structure. The excellent agreement for the $[10L]$ data shows the correctness of the model and also that the stacking of the atomic planes is well ordered.

This demonstrates that replacing the least-squares method by straightforward calculation of intensities on a grid of all of the adjustable parameters of the model works well for SLs with no stacking disorder. It gives the structure of the SL and there is a very good agreement between measured and calculated intensities both for $[00L]$ and for $[10L]$ reflections.

4. Structure of Co/Cu superlattices

Two samples of Co/Cu SLs with nominal compositions of $(Co_{24}/Cu_{24})_{50}$, SL I and SL II, have been investigated. They have a mosaic spreads of 0.75° and 0.82° respectively, as determined from the rocking curves of the central (main) SL peaks. Tables 1 and 2 list these and other structural parameters of the SLs. For a scattering vector $\boldsymbol{Q}$ parallel to the SL growth direction a series of satellites is observed, figures 3(a) and 3(b), indicating that there is a good SL structure in the growth direction. From the scans in the $[00L]$ direction through the (002) and (004) Bragg reflections the positions and intensities of the SL satellites were determined. This information enables us to find the average bilayer length $\overline{L}$ and the total number of atomic planes in a Co/Cu bilayer. The FWHM of the SL peaks was measured both in longitudinal [001] and transverse [100] directions versus the order of a satellite. The results are presented in figure 4 for sample II and show that the width does not increase with satellite order in either direction. This indicates [32, 42, 45, 46, 49] that there is no noticeable discrete fluctuation of the bilayer thickness (as this would broaden the satellites in the growth direction) or interface roughness (which would affect the rocking curves). We should note that the last conclusion about a smooth interface is of limited accuracy because both samples have a high mosaicity, which may hide any broadening associated with the roughness. The FWHM of the central peak in the [100] direction gives an in-plane domain size of 6.23(7) nm consistent with other results [32]. From the width of the central peak in the $[00L]$ direction we can obtain an estimate for the out-of-plane structural coherence length (CL) of the SL $\sigma = 2\pi/\mathrm{FWHM}$ and the results are given in table 1.

Scans were also performed with the scattering vector along the $[10.L]$ direction running between the $(220)_{\mathrm{f.c.c.}}$ and $(224)_{\mathrm{f.c.c.}}$ reflections (see figure 1(C)) and a fragment of the diffraction pattern covering one period of intensity is presented in figure 3(c). These scans show, figure 3(c), that there are no SL peaks in the diffraction pattern. However, the intensity distribution is quite complex. The peaks at $L = 50.238\ \mathrm{nm}^{-1}$ and $L = 80.143\ \mathrm{nm}^{-1}$ arise from the (113) and (224) reflections of Cu stacked in the ABCABC... arrangement and the peak at $L = 70.163\ \mathrm{nm}^{-1}$ is from the $(\overline{3}\overline{3}1)$ reflection of the twinned domain of f.c.c. Cu (with the reverse sequence of atomic planes, i.e. ACBACB...). The observation of two twinned domains is consistent with other measurements of Co/Cu SLs [3,31]. The data also show similar reflections from f.c.c. Co with ABC... stacking at $L = 51.639\ \mathrm{nm}^{-1}$ and $L = 81.911\ \mathrm{nm}^{-1}$ and from the twinned f.c.c. Co at $L = 71.941\ \mathrm{nm}^{-1}$. There is also strong scattering from the h.c.p. Co reflections (103), (104) and (105) at $L = 46.610\ \mathrm{nm}^{-1}$, $L = 61.789\ \mathrm{nm}^{-1}$ and $L = 77.531\ \mathrm{nm}^{-1}$. The numerical values are slightly different for the other sample, but the diffraction pattern is very similar. The positions of the peaks in the $[10L]$ direction give the d_{111} (f.c.c.) or d_{001} (h.c.p.) lattice spacings for each structure. The in-plane lattice constants were within error the same for Co and Cu, demonstrating a complete accommodation of the Co and Cu lattices in the plane. The coherence lengths of Co and Cu determined from the FWHM of the peaks in the $[10L]$ direction do not exceed the thickness of the individual layers and are listed in table 1. Since the structure factors of the f.c.c. and h.c.p. reflections are known, the

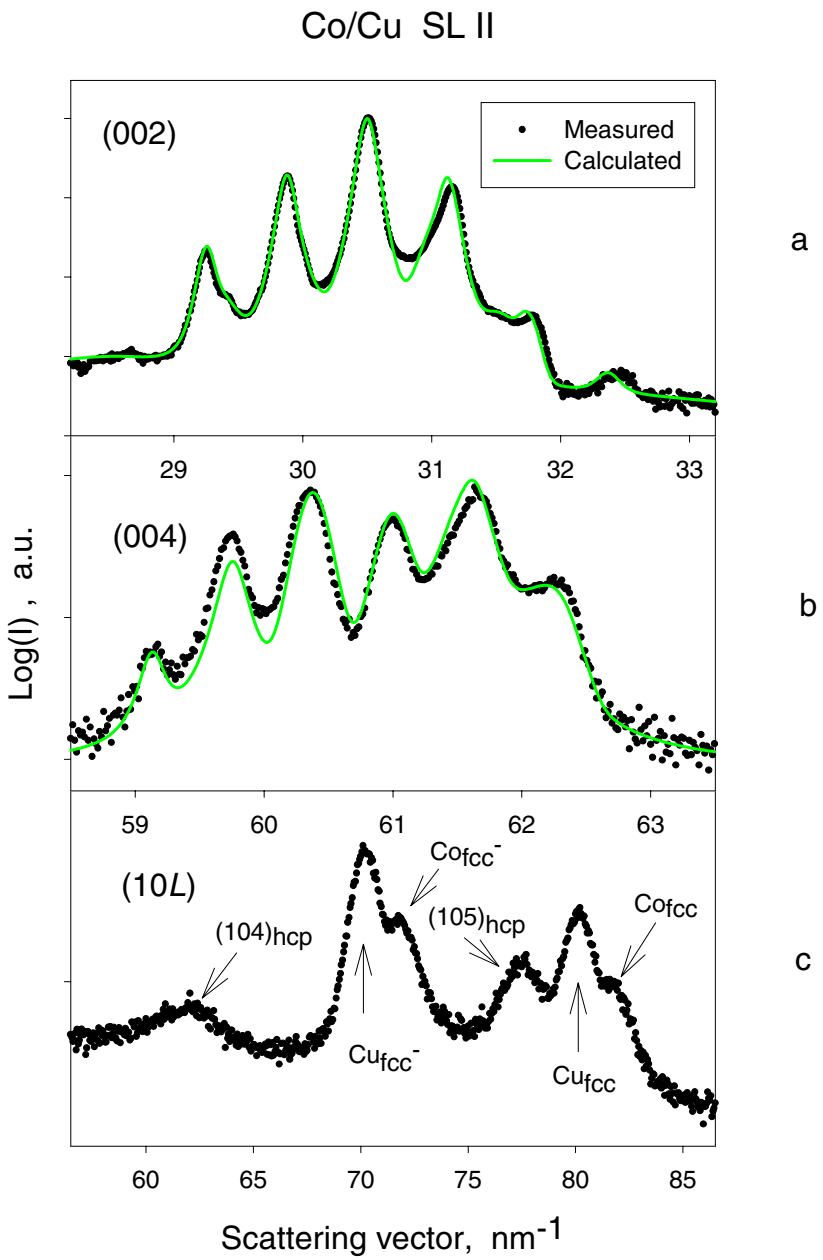

Figure 3. The x-ray scattering from SL II. Simulated x-ray diffraction profiles match well with the intensity distribution around the first- and second-order main Bragg reflections measured by [00*L*] scans ((a), (b)). The parameters of the model are given in table 2, for SL II, model A, and in the text. The scattering along [10*L*] is shown in (c) and contains reflections of f.c.c. and h.c.p. Co, f.c.c. Cu and of twinned f.c.c. Co and Cu shown as f.c.c.$^{-}$.

proportion of f.c.c. and h.c.p. phases can be determined from the measured intensities of the f.c.c. and h.c.p. reflections. The results for SL I show that 83% of Co is h.c.p. and only 17% is f.c.c. and the corresponding values for SL II are 80% and 20%.

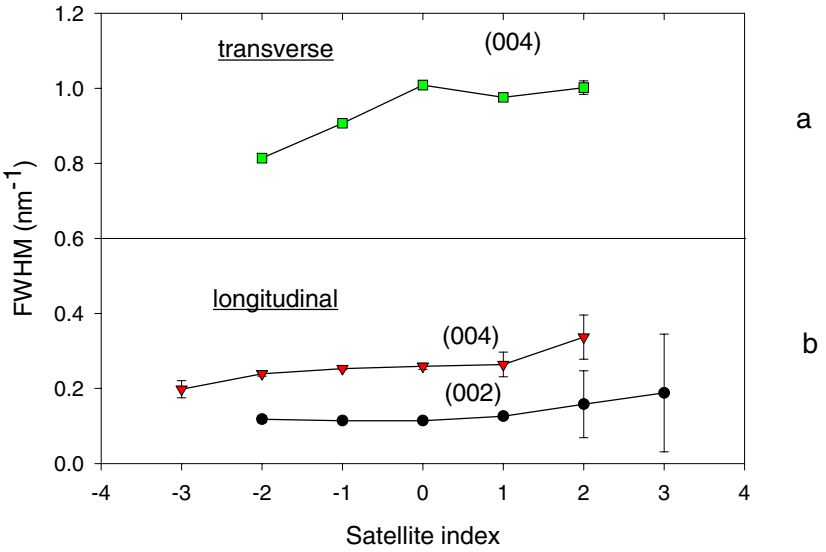

Figure 4. FWHM versus superlattice satellite index (SL II) measured in (a) transverse and (b) longitudinal scans.

The structure of the SLs can now be modelled taking into account the supplementary information revealed from the scans along the $[10L]$ direction. Since the Co layers are not uniform and contain two sets of planes, one with the h.c.p. stacking and the other with the f.c.c. stacking, the model developed in section 3 was modified. We have considered three different models which are shown schematically in figure 5: (A) the f.c.c. phase is a single block at the beginning of a Co layer; (B) two blocks of Cu f.c.c. phase are formed: one at the beginning and the other at the end of a Co layer with each block containing one half of the total number of cubic planes; (C) a single f.c.c. block forms in the middle of a Co layer. In each case the number of f.c.c. planes was rounded to the nearest integer and was equal to $0.83n_{\mathrm{Co}}$ (SL I) or $0.8n_{\mathrm{Co}}$ (SL II) as given by the amount of each structure calculated from the relative intensities of the h.c.p. and f.c.c. reflections. It was assumed that the lattice spacing remains equal to 0.208 77 nm (SL I) or 0.207 56 nm (SL II) throughout the whole f.c.c. block of Cu. Note that model A is consistent with the growth mechanism proposed previously [4, 5, 7, 8, 11, 28]. Model B includes the possibility of a change in the stacking of planes from h.c.p. to f.c.c. at the top of the Co layer [14].

The results are displayed in table 2 which gives the parameters for the SL obtained with each of the three models for SL I and SL II. Table 2 shows that for SL I each of the three models fits the data equally well while for SL II models A and B are equally good and it is difficult to judge which one is better from the values of the fit criteria R_{wp} and σ_{pos}. The block lengths (BLs) of f.c.c. Co, h.c.p. Co and f.c.c. Cu for both SLs are shown in table 2 and we can compare them with the measured out-of-plane CLs obtained from the measurements along the $[10L]$ direction (table 1). Model C shows less satisfactory agreement with the measured data in terms of BLs of the Cu layer. Moreover, the lattice spacings for Co and Cu layers calculated for models A and B match better than those for model C the measured d-spacings for both SLs (see tables 1 and 2). Therefore we conclude that model C does not give as good a description of the experimental data as models A and B and model C is excluded from further consideration.

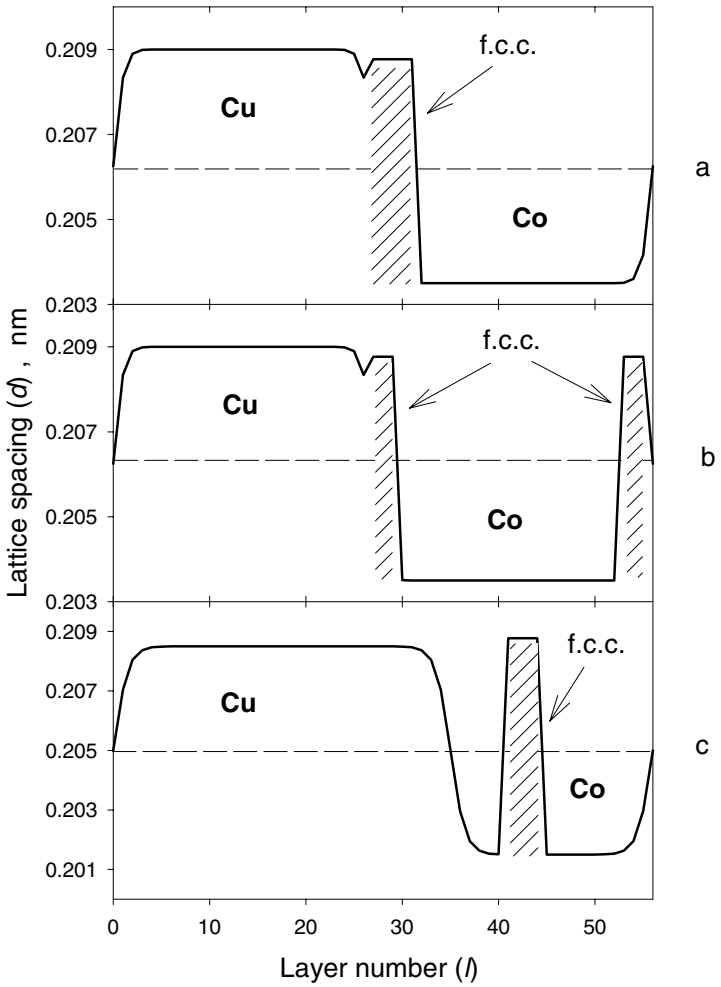

Figure 5. The variation of the d-spacing along the growth direction for three different models, (a) A, (b) B and (c) C, discussed in the text.

It is more difficult to decide whether model A or B is better. Model A gives a bigger BL of f.c.c. Co and probably provides the more realistic model of the SL structure. Otherwise the f.c.c. structure would occur only in the form of very thin (two or three atomic planes thick) lamellae which would give a broadening of the reflections of cubic Co in the $[10L]$ direction. The diffraction pattern in figure 3(c) and similar scans for SL I show no evidence of such broadening. Hence, model A which assumes that the Co layer consists of a single block of h.c.p. Co and a smaller block of f.c.c. Co gives the most adequate description of the experimental data.

To account for the effect of a possible variance of parameters we averaged the parameters of the best 30 SLs for model A generated by our fitting routine and the results are given in table 2. They show little difference between the best-fit model and the averaged one. This confirms that model A in table 2 does correspond to a well-defined minimum in parameter space.

The BL of f.c.c. Co in model A was 1.04 nm for SL I and 1.45 nm for SL II (see table 2). Both values are noticeably smaller than the CL of 4.06 nm and 4.25 nm measured for the

Table 1. Measured and calculated structural parameters of Co/Cu superlattices as determined by x-ray diffraction at room temperature.

Parameter		SL I	SL II
Mosaic spread (deg)		0.75(3)	0.82(4)
Average SL d-spacing (nm)		0.20654	0.20600
Average bilayer length $\overline{L}$ (nm)		11.31 ($\pm$0.26)	9.86 ($\pm$0.34)
Total number of atomic planes $N = n_{\mathrm{Co}} + n_{\mathrm{Cu}}$		56	49
In-plane lattice constants (nm):			
Co:	$a_{\mathrm{h.c.p.}}$		0.25352(19)
	$a_{\mathrm{f.c.c.}}$	0.35963(13)	0.35956(10)
Cu:	$a_{\mathrm{f.c.c.}}$		0.36009(40)
Out-of-plane lattice constants/lattice spacings (10.L scans) (nm):			
Co:	$a_{\mathrm{f.c.c.}}/d_{111}$	0.36160/0.20877	0.35950/0.20756
	$c_{\mathrm{h.c.p.}}/d_{001}$	0.40757/0.20379	0.40641/0.20321
Cu:	$a_{\mathrm{f.c.c.}}/d_{111}$	0.36269/0.20940	0.36392/0.21011
Out-of-plane SL coherence length ([00L] scans) (nm)		26 ($\pm$0.5)	55 ($\pm$0.5)
In-plane SL coherence length ([100] scans) (nm)			6.23(7)
Out-of-plane coherence length ([10L] scans) (nm)			
Co:	h.c.p.	2.20	2.58
	f.c.c.	4.06	4.25
Cu:	f.c.c.	4.71	4.36
Relative amount of h.c.p. and f.c.c. phase in Co bilayers (%)			
Co:	h.c.p.	83 ($\pm$10)	80 ($\pm$10)
Co:	f.c.c.	17 ($\pm$10)	20 ($\pm$10)

Table 2. The structural parameters of Co/Cu superlattices. The parameters given in the table were obtained from fits to the diffraction profiles made using the scattering model described in section 3. Model A corresponds to calculation made assuming a single block of f.c.c. structure. Model B includes two blocks of f.c.c. Co. Model C is with a f.c.c. block in the middle of the Co layer.

Number of planes		Lattice spacings (nm)		Interface parameter	Size of blocks (nm)			R_{wp}	σ_{pos}	Model
					Co		Cu			
n_1	n_2	d_1	d_2	λ_1	h.c.p.	f.c.c.	f.c.c.	(%)	(%)	No
SL I										
29	27	0.2035	0.2090	1	4.88	1.04	5.64	31.9	0.09	A
29	27	0.2035	0.2090	1	5.09	0.42	5.64	30.7	0.28	B
21	35	0.2015	0.2085	1.5	3.46	0.84	7.30	32.1	0.28	C
SL II										
34	15	0.2035	0.2105	4	5.49	1.45	3.16	16.2	0.13	A
32	17	0.2035	0.2100	4	5.29	0.62	3.57	15.9	0.11	B
17	32	0.2010	0.2080	4.5	2.85	0.62	6.66	56.3	0.02	C
Averaged over the best 30 models										
28.6(5)	27.4(5)	0.2035(0)	0.2090(0)	1.4(3)				34.5		SL I, A
33.0(9)	16.0(9)	0.2035(0)	0.2101(4)	3.4(6)				17.6		SL II, A

[10L] direction respectively (table 1). This may arise because we have assumed that every atomic plane is continuous. In fact, strong evidence exists that this is true only for relatively thick (>1 nm) Co layers because the first few monolayers of Co have been shown by NMR and LEED studies to form discontinuous islands [4, 6, 10–12]. If the same amount of f.c.c.

Co grows in islands, the CL in the [10L] direction will be higher and could approach the experimentally observed CL.

The CL of h.c.p. Co is much smaller than we would expect from the model BLs. The CL of cubic Co is almost twice the CL of a hexagonal one whereas there is considerably more of the hexagonal phase (table 1). The low CL of the hexagonal phase may be due to SFs which destroy the regular stacking of planes in hexagonal Co. It is known from the experiments on the bulk material that the concentration of SFs in the f.c.c. phase is usually very low both for pure Co and for Co alloys [35, 53, 54]. On the other hand, hexagonal Co is often disordered and the faults may change the stacking of 10% of the atomic planes [33, 35]. The CL of h.c.p. Co in our experiments is 11 (SL I) or 13 (SL II) close-packed planes, so the concentration of SFs is of the same order of magnitude as reported [33, 35] for bulk Co.

4.1. Structure of the Co/Cu superlattice after heating to 700 °C

The stability of a Co/Cu SL II was investigated by heating it quickly to 700 °C in UHV to avoid any oxidation, and cooling slowly to room temperature. Upon heating, the SL structure was completely destroyed. The diffraction patterns in figure 6 show two sets of reflections: one from f.c.c. Co ($a = 0.353\,53$ nm) and the other from Cu ($a = 0.365\,20$ nm); there are no SL peaks, there is no scattering from h.c.p. Co and there is no in-plane epitaxial matching. Both materials have f.c.c. domains of normal and twinned orientation, similar to the SLs discussed in section 4. The out-of-plane CL measured in the [00L] direction was found to be 56.6 nm for Cu and 61.0 nm for Co and these values are comparable to the CL of SL II before heating. Transverse scans through the centres of these reflections showed an increase of the in-plane CLs to 17.5 nm and 15.2 nm, respectively. The increase indicates that the planes became flatter upon heat treatment. This is probably due to separation of Co and Cu atoms taking place on slow cooling due to diffusion of both atoms away from mixed Co/Cu interfaces typical for strained SLs, as we have shown in the previous section. This behaviour is consistent with the equilibrium phase diagram of the Co–Cu system which predicts very low solubility of these materials at moderate and low temperatures.

5. Summary and discussion

We have presented the results of a high-resolution x-ray diffraction study of Co/Cu SLs grown by MBE. We have suggested replacing a standard least-squares fitting of parameters of SLs with a calculation of all possible models on a grid of parameter values and believe that this approach is more reliable. The method has been shown to give excellent results for a Dy/Lu superlattice. The advantage of the method is that it is often difficult to find new minima in parameter space with the conventional least-squares method and the direct method overcomes this problem.

We have applied the method to find the structure of Co/Cu SLs. Unexpectedly we found that 80–83% of the Co layer was in the h.c.p. phase and only 17-20% in the f.c.c. phase. This is in contrast to the case for the Co/Cu SLs grown similarly by Bödeker *et al* [31] who found no evidence for any h.c.p. Co phase. Their SLs were Co_{44}/Cu_{77} and Co_{34}/Cu_{20} whereas ours were Co_{29}/Cu_{22} and Co_{34}/Cu_{15}. Since our samples had Co layers thinner than or similar to theirs it is surprising that their samples had no h.c.p. Co phase whereas ours had a majority of Co in the h.c.p. phase. Our finding is also in contrast to the results of spin-resonance measurements by Thomson *et al* [55] who found that Co was predominantly in the f.c.c. phase with only a minor contribution from the h.c.p. phase to the spin-echo intensity.

The detailed models of the phases strongly suggest that when the Co is grown on Cu,

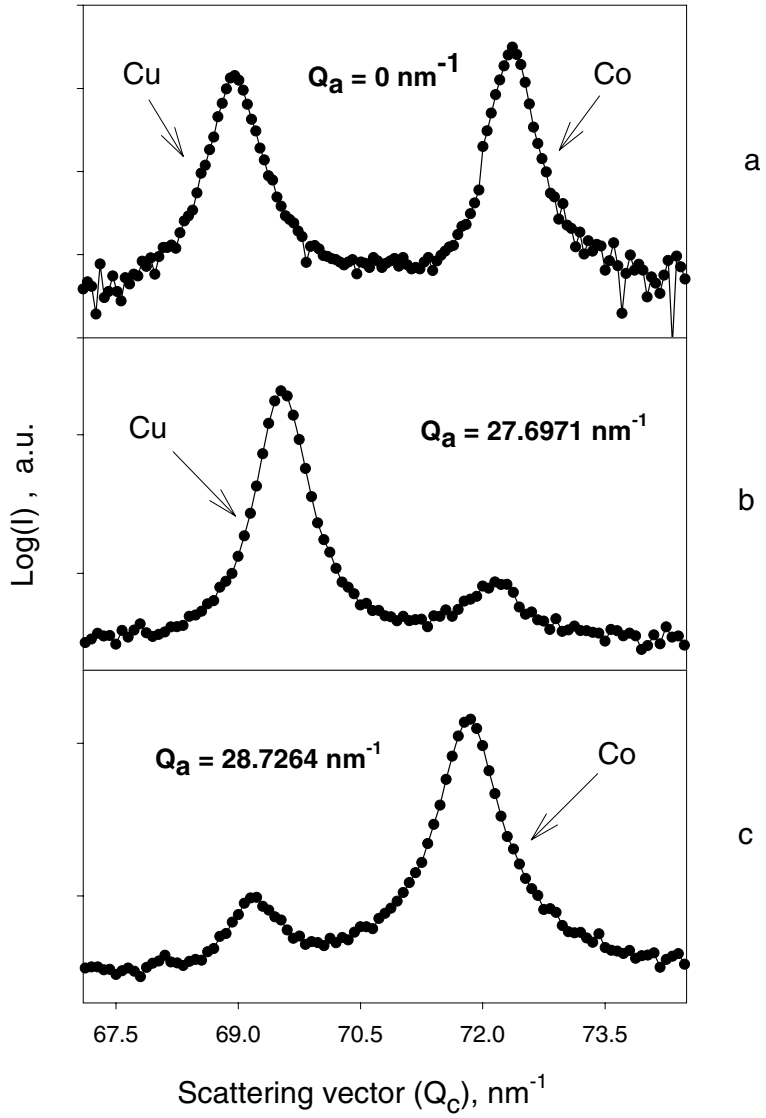

Figure 6. X-ray scattering from sample II after one cycle of heating to 700 °C and cooling down to 20 °C. Scattering along the [00L] (a) and [10L] ((b), (c)) directions shows no evidence of superlattice peaks and no in-plane epitaxial matching between the Co and Cu lattices.

it initially grows in f.c.c. islands but that the structure then becomes h.c.p. The Cu in contrast grows immediately in the f.c.c. phase. This is consistent with other data concerning the growth [4,5,7,8,11,14,22,28]. The interface widths are about three layers thick, showing that the growing surface is quite rough. This result is in agreement with a previous study [32] and the roughness is possibly due to the low growth temperature used.

The observations also show that the h.c.p. Co is 1-D disordered by SFs occurring after 11 to 13 perfectly stacked atomic planes. The degree of stacking disorder in the SLs is comparable to that for bulk Co [33,35] assuming a random distribution of SFs in the h.c.p. structure. Whether or nor the distribution of SFs is random is not completely clear and requires additional study.

The observation of a large fraction of h.c.p. Co in the Co layers, in contrast to the findings of other work on Co/Cu SLs, shows that further work is needed to control the structure of the Co layers. Since the details of the electron transport and exchange interactions between the Co layers are likely to depend on the Co crystal structure, reliable and reproducible data for the magnetic and magnetotransport properties will be obtained only when the structures are carefully controlled.

Acknowledgments

We would like to thank M R Wells and R C C Ward for growth of the Dy/Lu sample and for heat treatment of the samples, M A Howson for stimulating discussions and S Hemon for assistance with the experiments. This research was supported by a grant from the Engineering and Physical Sciences Research Council.

References

[1] Parkin S S P, Bhadra R and Roche K P 1991 *Phys. Rev. Lett.* **66** 2152
[2] Kano H *et al* 1993 *Appl. Phys. Lett.* **63** 2839
[3] Lamelas F J, Lee C H, He H, Vavra W and Clarke R 1989 *Phys. Rev.* B **40** 5837
[4] Meny C, Panissod P and Loloee R 1992 *Phys. Rev.* B **45** 12 269
[5] Tonner B P, Han Z-L and Zhang J 1993 *Phys. Rev.* B **47** 9723
[6] de la Figuera J, Prieto J E, Ocal C and Miranda R 1993 *Phys. Rev.* B **47** 13 043
[7] Kief M T and Egelhoff W F 1993 *Phys. Rev.* B **47** 10 785
[8] Hochstrasser M, Zurkirch M, Wetli E, Pescia D and Erbudak M 1994 *Phys. Rev.* B **50** 17 705
[9] Le Fevre P, Magnan H, Heckmann O and Chandesris D 1995 *Physica* B **208–209** 401
[10] Xu J *et al* 1997 *Phys. Rev.* B **55** 416
[11] Jedryka E, Wojcik M, Nadolski S, Kubinski D J and Holloway H 1998 *J. Magn. Magn. Mater.* **177–181** 1183
[12] Heinz K, Müller S and Hammer L 1999 *J. Phys.: Condens. Matter* **11** 9437
[13] Hase T P A *et al* 2000 *Phys. Rev.* B **61** R3792
[14] Prieto J E, Rath C, Müller S, Miranda R and Heinz K 1998 *Surf. Sci.* **401** 248
[15] Dang K L, Veillet P, Velu E, Parkin S S P and Chappert C 1993 *Appl. Phys. Lett.* **63** 108
[16] Xu J *et al* 1996 *J. Magn. Magn. Mater.* **156** 69
[17] Buckley M E, Hope S, Schumann F O and Bland J A C 1996 *J. Magn. Magn. Mater.* **156** 211
[18] Joyce D E *et al* 1998 *Phys. Rev.* B **58** 5594
[19] Laidler H and Hickey B J 1996 *J. Appl. Phys.* **79** 6250
[20] Hase T P A *et al* 1998 *J. Magn. Magn. Mater.* **177** 1164
[21] Schuller I K, Kim S and Leighton C 1999 *J. Magn. Magn. Mater.* **200** 571
[22] Shima M, Salamanca-Riba L, Moffat T P and McMichael R D 1999 *J. Magn. Magn. Mater.* **198–199** 52
[23] Kok K Y, Hall M J and Leake J A 1996 *J. Magn. Magn. Mater.* **156** 51
[24] Pape I, Hase T P A, Tanner B K and Wormington M 1998 *Physica* B **253** 278
[25] Parkin S S P 1992 *Appl. Phys. Lett.* **61** 1358
[26] Fujimoto T, Patel M, Bland J A C, Gu E and Daboo C 1996 *J. Magn. Magn. Mater.* **156** 365
[27] Levy P and Zhang S F 1996 *J. Magn. Magn. Mater.* **164** 284
[28] Jesser W A and Matthews J W 1968 *Phil. Mag.* **17** 461
[29] Gu T, Goldman A I and Mao M 1997 *Phys. Rev.* B **56** 6474
[30] de Bernabe A, Capitan M J, Fisher H E and Prieto C 1998 *J. Appl. Phys.* **84** 1881
[31] Bödeker P *et al* 1993 *Phys. Rev.* B **47** 2353
[32] Lamelas F J, He H D and Clarke R 1991 *Phys. Rev.* B **43** 12 296
[33] Edwards O S and Lipson H 1942 *Proc. R. Soc.* A **180** 268
[34] Frey F, Prandl W, Schneider J, Zeyen C and Ziebeck K 1979 *J. Phys. F: Met. Phys.* **9** 603
[35] Frey F and Boysen H 1981 *Acta Crystallogr.* A **37** 819
[36] Nabarro F R N 1967 *Theory of Crystal Dislocations* (Oxford: Clarendon)
[37] Betteridge W 1979 *Prog. Mater. Sci.* **24** 51
[38] Dillamore I L, Smallman R E and Roberts W T 1964 *Phil. Mag.* **9** 517
[39] Babkevich A Y, Frey F, Neder R and Nikolin B I 1996 *Phys. Status Solidi* a **155** 3

[40] Bröhl K, Bödeker P, Metoki N, Stierle A and Zabel H 1993 *J. Cryst. Growth* **127** 682
[41] *International Tables for Crystallography* 1995 vol C, ed A J C Wilson (Dordrecht: Kluwer Academic) ch 9.2, pp 660–7
[42] Clemens B M and Gay J G 1987 *Phys. Rev.* B **35** 9337
[43] Locquet J-P, Neerinck D, Stockman L, Bruynseraede Y and Schuller I K 1988 *Phys. Rev.* B **38** 3572
[44] Locquet J-P, Neerinck D, Stockman L, Bruynseraede Y and Schuller I K 1989 *Phys. Rev.* B **39** 13 338
[45] Fullerton E E, Schuller I K, Vanderstraeten H and Bruynseraede Y 1992 *Phys. Rev.* B **45** 9292
[46] McMorrow D F, Swaddling P P, Cowley R A, Ward R C C and Wells M R 1996 *J. Phys.: Condens. Matter* **8** 6553
[47] Sevenhans W, Gijs M, Bruynseraede Y, Homma H and Schuller I K 1986 *Phys. Rev.* B **34** 5955
[48] Speriosu V S and Vreeland T 1984 *J. Appl. Phys.* **56** 1591
[49] Chrzan D and Dutta P 1986 *J. Appl. Phys.* **59** 1504
[50] Jehan D A *et al* 1993 *Phys. Rev.* B **48** 5594
[51] McCusker L B, Dreele R B V, Cox D E, Louër D and Scardi P 1999 *J. Appl. Crystallogr.* **32** 36
[52] *PeakFit User's Manual* 1995 Jandel Scientific, San Rafael, CA 94901, USA (peak separation and analysis software for Windows)
[53] Nikolin B I 1983 *Scr. Metall.* **17** 699
[54] Nikolin B I, Babkevich A Y, Sizova T L and Shevchenko N N 1988 *Scr. Metall.* **22** 761
[55] Thomson T, Riedi P C, Wellock K P and Hickey B J 1997 *J. Appl. Phys.* **81** 4469